Preprints, Joint 9th IFAC Symposium on Robust Control Design and
2nd IFAC Workshop on Linear Parameter Varying Systems
Florianopolis, Brazil, September 3-5, 2018

LPV Control of a Gyroscope with Inverted Pendulum Attachment

P.J.W. Koelewijn * **P.S.G. Cisneros** ** **H. Werner** **
R. Tóth *,⋆

* *Eindhoven University of Technology, Eindhoven, The Netherlands, (e-mail: p.j.w.koelewijn@student.tue.nl; r.toth@tue.nl).*
** *Hamburg University of Technology, Hamburg, Germany, (email: pablo.gonzalez@tuhh.de; h.werner@tuhh.de).*

Abstract: *A linear parameter varying* (LPV) optimal $\mathcal{L}_2$ gain controller is designed with mixed-sensitivity shaping to stabilize an inverted pendulum attached to a *control moment gyroscope* (CMG). Swing-up of the pendulum is achieved by a start-up LPV controller for which the reference is designed by an energy regulator. The LPV performance controller is enabled as soon as the pendulum enters into its operating range of ± 0.15 rad. Based on both simulation and experimental results, it is demonstrated that stabilization of the pendulum is achieved for varying gimbal angles and rotational speed of the flywheel.

Keywords: Linear parameter-varying, optimal control, control moment gyroscope, pendulum, mixed sensitivity.

1. INTRODUCTION

Control moment gyroscopes (CMGs) are used in various applications, e.g. for attitude control in spacecrafts (Kristiansen et al. (2005)). From a dynamical aspect, CMGs correspond to coupled nonlinear systems with challenging rotational dynamics affected by friction and pose dependent disturbances due to manufacturing imperfections. Hence, they are often used as a test-bed for nonlinear controller design, e.g., see Reyhanoglu and van de Loo (2006). Attaching an inverted pendulum to one of the gimbals makes the already nonlinear coupled CMG even more complex, raising the question how a reliable nonlinear controller can be designed for this application in a simple systematic manner.

Over the last decades, significant research has been devoted to the development of the *linear parameter-varying* (LPV) system theory resulting in numerous publications and case studies, see, e.g., Rugh and Shamma (2000), Scherer (2001), Hoffmann and Werner (2015). The principle idea behind of the LPV approach is to address nonlinear controller design in a systematic, linear framework. This framework can be seen as an extension of the *linear time-invariant* (LTI) system theory. The purpose of the current paper is to demonstrate how LPV control can be applied and implemented on the challenging stabilization problem of the pendulum attached CMG and to analyse the performance of the resulting controlled system using both simulation and empirical studies.

Our work can be seen as a continuation of previous studies of LPV control on the CMG which have shown significant performance improvements compared to LTI control methods, see Abbas et al. (2013), Abbas et al. (2014), and Theis et al. (2014). By our knowledge, application of LPV control on the CMG with inverted pendulum has not been investigated yet. Furthermore, compared to the previous works, we propose a scheme in which the complex task of swing-up and stabilization of a CMG-actuated inverted pendulum is divided into simpler tasks to enable design of simpler controllers, thereby improving tractability of the synthesis conditions and achieving better performance for this complex system. One LPV controller is designed for swing-up with an energy based computation of its reference trajectory. While for stabilization, a separate high-performance LPV controller is synthesized. For LPV controller synthesis, the LPVTools Toolbox for MATLAB was used, Hjartarson et al. (2015).

The structure of the paper is as follows: in Section 2, a description of the plant is given and it is explained how its motion dynamics can be expressed with an LPV model. In Section 3, the control objectives and the utilized LPV controller design is explained. This is followed by Section 4, where the performance of the control structure is assessed and demonstrated in both simulation-based and experimental studies. Finally in Section 5, concluding remarks are briefly presented.

Notation: $\mathrm{diag}(A_1, \ldots, A_n)$ indicates a (block) diagonal matrix with square matrix entries A_1,...,A_n along the diagonal. The notation $A \succ 0$ ($A \succeq 0$) indicates that A is symmetric and positive (semi)definite, while $A \prec 0$ ($A \preceq 0$) indicates that A is symmetric and negative (semi)definite. The identity matrix of size N is denoted by I_N.

2. PLANT MODEL

2.1 Plant description

The plant that is used is an ECP model 750 CMG, (Educational Control Products (1999)), with the A51 inverted pendulum accessory, (Educational Control Prod-

⋆ This work has received funding from the European Research Council (ERC) under the European Unions Horizon 2020 research and innovation programme (grant agreement No 714663).

Copyright © 2018 IFAC

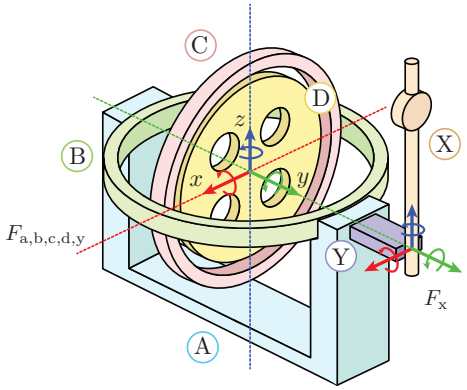

Fig. 1. Schematics of the CMG with the inverted pendulum attachment.

ucts (2003)). This system is modelled in terms of bodies A, B, C, D, X and Y, see Fig. 1. Body D is a disk (flywheel) with rotation angle q_1 around the y-axis in frame F_d. This disk is actuated by a motor with an applied torque τ_1 aligned with the positive direction of q_1. Body C with a rotation angle q_2 around the x-axis in frame F_c is the gimbal encompassing the disk. Body C is also actuated in terms of a motor with generated torque τ_2 applied in the positive direction of q_2. Body B is the gimbal encompassing gimbal C which is locked in the position shown in Fig. 1 (i.e. $q_3 \equiv 0$) for this setup; this is necessary, since the encoder of the pendulum replaces the encoder of body B. Body A is the gimbal encompassing body B with rotation q_4 in the positive direction around the z-axis in frame F_a. Body Y is the attached plate of the inverted pendulum and is modelled as an inertia attached to body A. The frames of references for bodies A, B, C, D and Y are all centred at the middle of body A, but attached to their respective body. Finally, body X is the inverted pendulum attached to body A with rotation q_x in the positive direction around the y-axis in frame F_x. Frame F_x is attached to the pendulum. The angular velocities of the disk, gimbals and pendulum are denoted by ω_1, ω_2, ω_4 and ω_x respectively. The friction can be assumed to be viscous between all the different connected axis in the form of $f_{v,*}\omega_*$. All rotational angles are measured by incremental encoders.

2.2 Nonlinear model

Due to the complex dynamics of both the CMG and the inverted pendulum, it was chosen to use the Neweul-M^2 software package for MATLAB, Kurz et al. (2010), to model the system. Using Neweul-M^2 the equations of motion can be generated which are of the form

$$\mathbf{M}(q,t)\ddot{q}(t) + \mathbf{K}(q,\dot{q},t) = \mathbf{F}(q,\dot{q},t) + \mathbf{B}u(t) \qquad (1)$$

where $q = [q_1\ q_2\ q_3\ q_4\ q_x]^T$, $u = [\tau_1\ \tau_2]^T$, $\mathbf{M}$ is the generalized mass matrix, $\mathbf{K}$ is the vector of the generalized Coriolis, centrifugal, and gyroscopic forces, $\mathbf{F}$ is the vector of generalized forces, and $\mathbf{B}$ is the input matrix. Equation (1) can be rewritten as a nonlinear state-space model:

$$\dot{x}(t) = f(x(t),u(t)), \qquad (2)$$

where $x = \begin{bmatrix} q^T & \dot{q}^T \end{bmatrix}^T$ is the state, u is the input and

$$f(x(t),u(t)) = \begin{bmatrix} \dot{q}(t) \\ \mathbf{M}^{-1}(x(t))\Big(\mathbf{F}(x(t)) - \mathbf{K}(x(t)) + \mathbf{B}u(t)\Big) \end{bmatrix}.$$

The physical parameters of the system, such as inertias and frictions, were experimentally identified in Abbas et al. (2013). The inertias of the inverted pendulum were obtained from Educational Control Products (2003), other parameters of the pendulum were either experimentally identified or measured and are given in Table 1.

Table 1. Parameters of the inverted pendulum.

Parameter:	Friction coefficient	Pendulum mass
Variable:	$f_{v,x}$	M_x
Value:	1.87e-4	0.143
Unit:	Nm·(rad/s)$^{-1}$	kg
Parameter:	Pendulum arm length	Distance F_a to F_x
Variable	L	R
Value:	0.267	0.380
Unit	m	m

2.3 LPV model

To develop an LPV model of the nonlinear equations (2), a local modelling method is applied via a first order Taylor series expansion around the moving operating point of (2), the same method is applied in Abbas et al. (2013) and Abbas et al. (2014) for the CMG without inverted pendulum. Neweul-M^2 can directly compute such a linearisation over (x,u). Based on (2), it follows that the linearisation is only dependent on:

$$\rho = [q_2\ q_x\ \omega_1\ \omega_2\ \omega_4\ \omega_x]^T,$$

a subset of the variables in (x,u), and due to its analytical form, it can be directly used to approximate (2) as

$$\dot{x}(t) \approx A(\rho(t))x(t) + B(\rho(t))u(t). \qquad (3)$$

The high scheduling order of the LPV model in (3) leads to intractability of gridding-based controller synthesis for (3). In Abbas et al. (2014) a similar LPV model was derived and validated for the same CMG, albeit without inverted pendulum, and was used for LPV controller design. The LPV model in Abbas et al. (2014) uses as scheduling variables ω_1, q_2 and q_3 (recall that $q_3 = 0$ in this set-up). Various combinations of scheduling variables other than only q_2 and ω_1 were also investigated, but these did not result in significant changes in the singular value plots of frequency responses of the model for frozen values of ρ.

In line with the above given observations two different LPV models of the plant are now given: one used for synthesis of a swing-up controller and one for the design of a stabilizing controller (see Section 3 for the control structure). Because the states corresponding to the angles q_1 and q_2 do not influence the IO map, they can be truncated from the system.

Both LPV models are of the following form

$$\begin{aligned} \dot{x}_*(t) &= A_*(\rho(t))x(t) + B_*(\rho(t))u(t) \\ y_*(t) &= C_*x(t), \end{aligned} \qquad (4)$$

where, in the case of the stabilizing controller,

$$x_{st} = [q_4\ q_x\ \omega_1\ \omega_2\ \omega_4\ \omega_x]^T,$$

$$u = [\tau_1\ \tau_2]^T, \quad \rho_{st} = [q_2\ \omega_1]^T, \quad C_{st} = \begin{bmatrix} I_3 & 0 & 0 \\ 0 & 0 & I_2 \end{bmatrix},$$

and for the swing-up controller,

$$x_{sw} = [q_4\ \omega_1\ \omega_2\ \omega_4]^T,$$

$$u = [\tau_1\ \tau_2]^T, \quad \rho_{sw} = [q_2\ \omega_1]^T, \quad C_{sw} = \begin{bmatrix} I_2 & 0 & 0 \\ 0 & 0 & 1 \end{bmatrix}.$$

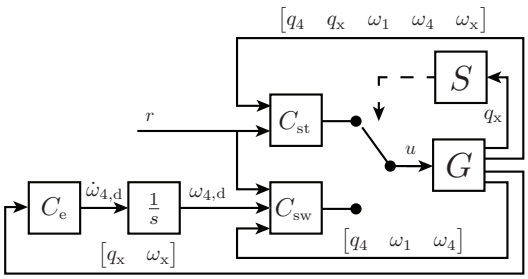

Fig. 2. Control structure: G is the plant, S is the switching logic, C_{st} is the LPV controller for stabilization, C_{sw} is the LPV controller for swing-up, and C_e is the energy-based regulator used during swing-up.

For the LPV controller used during swing-up, it is implicitly assumed that the effect of the pendulum on the dynamics of the CMG is negligible. Effects of the pendulum will now act as a disturbance on the system which can, to an extent, be taken care of by appropriate controller design. Both LPV models contain angular velocities in the output that are not directly measured in the real plant. These angular velocities are obtained via an appropriately designed differentiation filter.

3. CONTROLLER DESIGN

3.1 Control structure

The used control structure to achieve swing-up and stabilization consists of two separate control loops, one for swing-up and one for stabilization, in order to achieve better performance, especially for stabilization. The control structure is as follows:

- Swing-up is achieved by using a cascaded structure. The outer loop is based on an energy-based regulator C_e which computes the necessary angular acceleration $\dot{\omega}_4$ to swing-up the pendulum. This reference signal is integrated to compute a reference angular velocity ($\omega_{4,d}$) which is fed to the inner velocity LPV controller C_{sw}. An LPV controller is needed for this loop because these dynamics still depend on the gimbal angle q_2 and the angular velocity of the disk ω_1.
- Near the unstable equilibrium position, $q_x = 0$, a switching logic S switches control authority to a stabilizing controller C_{st} whose task it is to stabilize the pendulum and reject possible disturbances.

Linear switching strategies similar to the one used here have been used for a long time (Malmborg et al. (1996)) and have become a standard method for swing-up and stabilization of inverted pendulums. However, due to the complex nature of the CMG, a more advanced LPV extension of these control strategies is necessary for swing-up and stabilization. The chosen controller structure can be seen in Fig. 2. Note, for implementation the measured signal q_x was wrapped to $[-\pi, \pi]$.

First the general LPV controller design used for both the swing-up and stabilizing LPV controllers is explained, including individual design decisions for the swing-up and stabilizing LPV controllers. After that, the energy-based regulator is explained, and finally, the switching logic is shortly discussed.

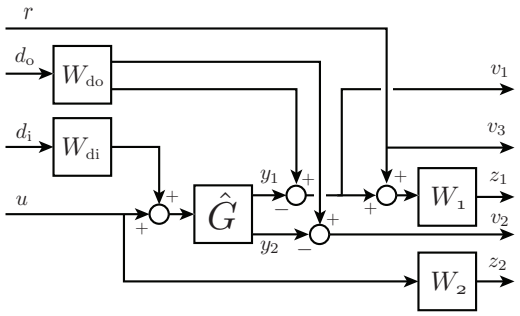

Fig. 3. General mixed sensitivity design used for both swing-up and stabilizing LPV controller synthesis.

3.2 LPV controller design

The synthesis of the LPV output feedback controller used for both swing-up and stabilizing LPV controller design is based on the method detailed in Wu (1995).

Considering a generalized plant of the form

$$\begin{bmatrix} \dot{\eta} \\ z \\ v \end{bmatrix} = \left[\begin{array}{c|cc} A(\rho) & B_w(\rho) & B_u(\rho) \\ \hline C_z(\rho) & D_{zw}(\rho) & D_{zu}(\rho) \\ C_v(\rho) & D_{vw}(\rho) & 0 \end{array}\right] \begin{bmatrix} \eta \\ w \\ u \end{bmatrix} \tag{5}$$

where z is the performance channel, w the disturbance channel, u the control input, v the measured outputs, η the state vector and ρ the scheduling variable. Using the synthesis method in Theorem 4.3.2 of Wu (1995) a stabilizing controller can then be found of the form

$$\begin{bmatrix} \dot{\xi} \\ u \end{bmatrix} = \begin{bmatrix} A_K(\rho, \dot{\rho}) & B_K(\rho, \dot{\rho}) \\ C_K(\rho, \dot{\rho}) & D_K(\rho, \dot{\rho}) \end{bmatrix} \begin{bmatrix} \xi \\ v \end{bmatrix}. \tag{6}$$

Both LPV controllers are designed using the four-block mixed-sensitivity loop shaping technique (Sefton and Glover (1990)). The generalized plant for the design can be seen in Fig. 3, where $\hat{G}$ is the scaled plant (scaled according to maximum allowable or expected input/output changes). The scaling for the input follows from the maximum torque the motors can deliver which is 0.666 Nm for τ_1 and 2.44 Nm for τ_2. In addition to weighting filters to describe the expected behaviour of the disturbances for improved disturbance rejection and robustness, a two degree of freedom structure was chosen to achieve improved tracking performance. For both the swing-up and the stabilizing LPV controller, the scheduling region is considered to be: $q_2 \in [-60°, 60°]$ and $\omega_1 \in [30 \text{ rad/s}, 60 \text{ rad/s}]$ and with the rate bound $\dot{q}_2 \in [-2 \text{ rad/s}, 2 \text{ rad/s}]$ and $\dot{\omega}_1 \in [-10 \text{ rad/s}^{-2}, 10 \text{ rad/s}^{-2}]$.

Swing-up controller: For the LPV controller C_{sw} used during swing-up, the outputs ω_4 and ω_1 (signal y_1 in Fig. 3) are scaled with 1.5 rad/s and 10 rad/s respectively ($\hat{G}$ in Fig. 3). The shaping filters are chosen as $W_1 = \text{diag}(W_{\omega_1}, W_{\omega_4})$, with each W_* having low pass characteristics thereby ensuring integral action and good tracking performance at low frequencies. For $W_2 = \text{diag}(W_{\tau_1}, W_{\tau_2})$, filters with high pass characteristics are chosen to enforce roll-off at high frequencies. The output of the generalized plant is augmented with $y_2 = q_4$ in order to regulate the angle q_4 to the neutral position in the swing-up phase. The disturbance filters are taken as constants $W_{di} = \text{diag}(0.5, 1.5)$ and $W_{do} = 0.1I_3$. Fig. 4 shows the sensitivity and control sensitivity plots for various frozen values of ρ in the scheduling region together with the inverse shaping

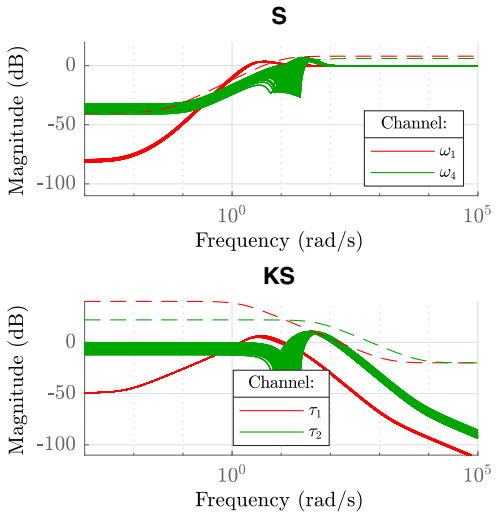

Fig. 4. Inverse weighting filters (dashed) and the frozen closed loop output sensitivity and control sensitivity magnitude plots (solid) for the individual channels of the swing-up LPV controller.

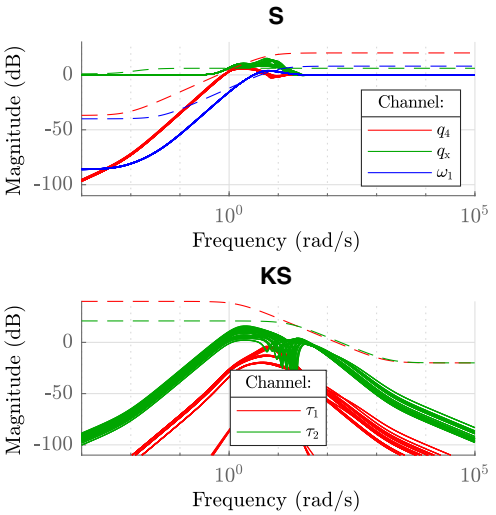

Fig. 5. Inverse weighting filters (dashed) and the frozen closed loop output sensitivity and control sensitivity magnitude plots (solid) for the individual channels of the stabilizing LPV controller.

filters for the LPV controller C_{sw}. Synthesizing the LPV controller using these weighting filters results in a $\mathcal{L}_2$-gain of 10.5, this large gain is due to the inclusion of q_4 in the output. As it can be seen in Fig. 4, the corresponding closed-loop output sensitivities and control sensitivities are close to the weighting filters.

Stabilizing controller: For the stabilizing controller C_{st}, the outputs q_4, q_{x} and ω_1 (signal v_1 in Fig. 3) are scaled with 45°, 10° and 10 rad/s respectively ($\hat{G}$ in Fig. 3). In order to add damping to the closed-loop response, the output of the generalized plant is augmented such that $v_2 = [\omega_4 \ \omega_{\text{x}}]^{\text{T}}$. Note that these signals are not part of the performance channel and are therefore not considered for the tracking objective. In this case, $W_1 = \text{diag}(W_{q_4}, W_{q_{\text{x}}}, W_{\omega_1})$ and W_2 shares the structure of the swing-up controller design. The disturbance filters are once again chosen constant, $W_{\text{di}} = \text{diag}(0.5, 1)$ and $W_{\text{do}} = 0.1I_5$. Fig. 5 depicts the inverse shaping filters W_1, W_2 together with the resulting sensitivity and control sensitivity for various frozen values of ρ in the scheduling region. Synthesizing the LPV controller using these weighting filters results in a $\mathcal{L}_2$-gain of 1.47.

In order to synthesize the controllers, the LPVTools MATLAB toolbox, Hjartarson et al. (2015) was used. A gridded method was used to solve the synthesis problem where the scheduling parameters are gridded in a 5×7 grid on q_2 and ω_1. For synthesis, the functional dependency of the parameter dependent matrices X and Y, characterizing the quadratic performance/stability, needs to be chosen. An affine dependency was chosen for simplicity for both the swing-up and stabilizing controller synthesis: $X(\rho) = X_0 + X_1\omega_1 + X_2 q_2$ and $Y(\rho) = Y_0 + Y_1\omega_1 + Y_2 q_2$.

Given that the LPV output feedback controllers depend both on $\rho = [q_2 \ \omega_1]^{\text{T}}$ and $\dot{\rho} = [\omega_2 \ \dot{\omega}_1]^{\text{T}}$ and because ω_1 is already obtained through a differentiating filter, dependency on $\dot{\omega}_1$ is dropped to avoid issues arising from further differentiation of the signals. On the other hand, ω_2 is obtained by using the aforementioned differentiation filter on q_2. For the differentiation filters the cutting frequency was set to 30 Hz.

3.3 Energy-based regulator

As previously explained, in order to do the swing-up of the inverted pendulum, a cascaded structure is chosen consisting of an outer energy-based regulator C_{e} and an inner velocity LPV controller C_{sw}. The energy-based regulator computes the required angular acceleration, $\dot{\omega}_4$, to decrease the total energy of the pendulum subsystem (i.e. to swing-up the pendulum), this signal is then integrated to obtain a reference for ω_4 for the swing-up LPV controller to track. The energy-based regulator is based on Åström and Furuta (2000) and designed as follows: using the Lagrange method, the equations of motion of the pendulum subsystem can be derived to be

$$M_{\text{x}}L^2\dot{\omega}_{\text{x}} - M_{\text{x}}LR\dot{\omega}_4\cos(q_{\text{x}}) - M_{\text{x}}gL\sin(q_{\text{x}}) = 0, \quad (7)$$

where M_{x} denotes the mass of the pendulum, L is the length of the pendulum arm, R is the radius from the pendulum to the centre of the CMG, and g is the gravitational acceleration. The total energy of the pendulum is given by

$$E = \frac{1}{2}M_{\text{x}}L^2\omega_{\text{x}}^2 + M_{\text{x}}gL(\cos(q_{\text{x}}) - 1). \quad (8)$$

To control this energy, the Lyapunov function candidate

$$V = \frac{1}{2}(E - E_0)^2, \quad (9)$$

is chosen, where E_0 is the total energy in the upright position. Computing the time derivative of the Lyapunov function results in

$$\dot{V} = (E - E_0)\omega_{\text{x}}M_{\text{x}}LR\dot{\omega}_4\cos(q_{\text{x}}), \quad (10)$$

which should be negative so that $V \to 0$ and $E \to E_0$. Assuming we can control $\dot{\omega}_4$, choosing it equal to

$$\dot{\omega}_4 = k_1(E - E_0)\omega_{\text{x}}\cos(q_{\text{x}}), \quad (11)$$

where k_1 is a tuning parameter, yields that

$$\dot{V} = k_1 M_{\text{x}}LR\left((E - E_0)\, w_{\text{x}}\cos(q_{\text{x}})\right)^2, \quad (12)$$

which is always negative for $k_1 < 0$. The energy in the upright position of the pendulum is equal to zero, therefore $E_0 = 0$.

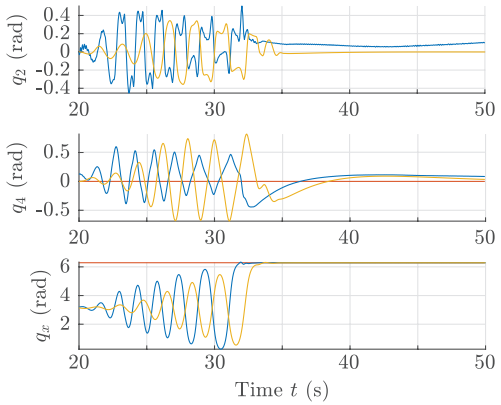

Fig. 6. Behaviour of the gimbal and pendulum angles during swing-up and stabilization; —— reference, —— experimental result, and —— simulation using the control structure in Fig. 2.

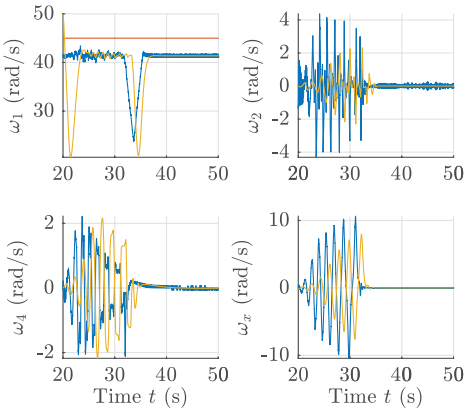

Fig. 7. Behaviour of the angular velocities of the gimbal and the pendulum during swing-up and stabilization; —— reference, —— experimental result, and —— simulation using the control structure in Fig. 2.

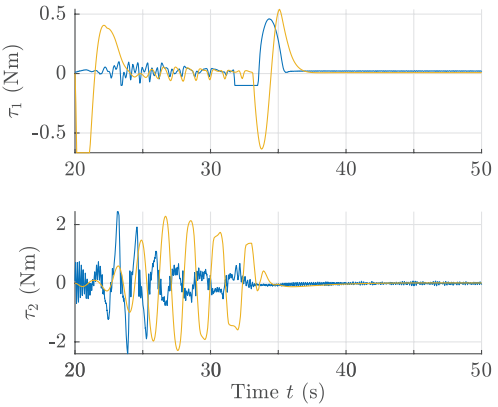

Fig. 8. Control input signals during swing-up and stabilization; —— experimental result, and —— simulation using the control structure in Fig. 2.

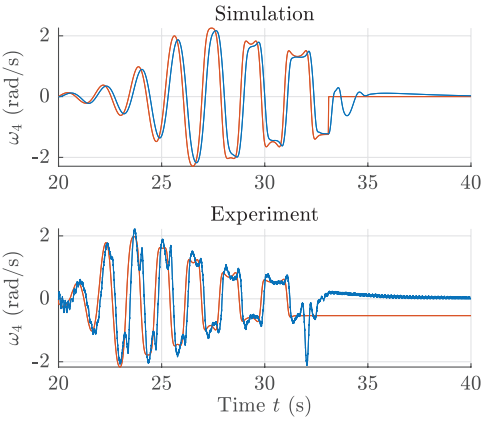

Fig. 9. Reference generated by the energy-based regulator and measured ω_4; —— reference, —— actual ω_4 using the control structure in Fig. 2 during swing-up.

Due to limited bandwidth of C_{sw}, the output of the energy-based regulator is not tracked perfectly. The energy of the pendulum subsystem is, in reality, not exactly described by (8). This causes the pendulum not to swing-up completely using the described structure. In order to compensate for this discrepancy, a tuning parameter (k_2) was added to the calculation of the kinetic energy (8) resulting in

$$E = k_2 \frac{1}{2} M_{\text{x}} L^2 \omega_{\text{x}}^2 + M_{\text{x}} g L(\cos(q_{\text{x}}) - 1). \qquad (13)$$

Where k_2 (in combination with k_1) was then used to fine tune how fast and how far the pendulum would swing-up, making sure it would not overshoot, but get sufficiently close to the upright position. For the simulation studies, these tuning parameters were set to $k_1 = -4$ and $k_2 = 1.03$; for the experiment, $k_1 = -4$ and $k_2 = 1$ were used.

3.4 Switching logic

In order to stabilize the pendulum in the upright position, control authority needs to switch from the cascaded loop (using the energy-based regulator and LPV velocity controller) to the stabilizing LPV controller. To accomplish this, a switching logic was implemented which smoothly switches the system to the stabilizing controller when the angle of the pendulum is close to zero. The angle at which the switch happens, $|q_{\text{x}}| < 0.15$ rad, was found by heuristically tuning the switching angle until a desired response was achieved. Smooth transition is achieved by using a ramp weighting of the output of both controllers. This is done by taking a convex combination of control input of both the swing-up and the stabilizing LPV controller during the transition. To avoid wind-up effects in the controller states, the controller is switched off and its states are reset when not being used. More advanced switching strategies, such as bumpless switching, could be used to lessen the effects of switching between two control loops.

4. SIMULATION AND EXPERIMENTAL RESULTS

To demonstrate the performance of the above detailed control structure and the designed controller, both simulation based and experimental studies have been conducted, which will be presented and discussed in this section.

For the experimental study, the disk was first sped up to 45 rad/s using a PI controller. After that, a small pulse is given to the swing-up controller in order to make the pendulum velocity larger than zero (otherwise (11) would stay zero and swing-up would not start). Then the system is switched to the described control structure to initiate swing-up and stabilization. In both simulation and experiment, a sampling time of 0.884 ms was used, which is the default sampling time of the CMG set-up. In Fig. 6 to

Fig. 9, the behaviour of the gimbal and pendulum angles and their angular velocities with the generated control inputs is depicted during swing-up and stabilization in both simulation and experiment.

In the figures, it can be seen that in the simulation and during the experiment, swing-up and stabilization was achieved. The swing-up is achieved in both cases in approximately 10 seconds. Similar behaviour for swing-up and stabilization has been observed both in simulation and in experiment. A noteworthy difference between experiment and simulation is the fact that q_2 does not stay close to zero in the experiment (cf. Fig. 6). This is likely caused by unmodeled friction effects not captured in the simulation model coupled with the fact that the state q_2 was eliminated from the state vector for both LPV controllers and is, therefore, not being regulated. One potential negative effect of not regulating q_2 is that it could leave the specified parameters bounds, thereby potentially causing instability. This was however never seen while carrying out the experiments.

Fig. 7 shows that there is a drop in ω_1 when the pendulum stabilizes, this is caused switching from the swing-up to the stabilizing LPV controller. Implementing bumpless switching between the swing-up and the stabilizing LPV controller could alleviate this issue, but it was not implemented in this study. Having the velocity controlled externally could also compensate for this, although this would not bring the benefits of also controlling τ_1. Note that ω_1 has a relatively large steady-state error. This is due to allowing large deviations in order to give ω_1 more freedom, because tighter control of ω_1 would allow ω_1 to deviate less, therefore worsening disturbance rejection and swing-up speed. Given that ω_1 is a scheduling parameter, the exact control of the disk speed is also not required.

Looking at the generated control inputs by the controllers in Fig. 8 it can be seen that for both simulation and experiment, the requested torques from the motors do not saturate, indicating an appropriate tuning of the control sensitivity. In Fig. 9, the reference generated by the energy-based regulator is depicted and the resulting ω_4 due to the tracking of the swing-up controller. It can be seen that, for both the simulation and the experimental study, ω_4 is tracked, albeit with a delay.

Video footage of the experiment can be found at `https://youtu.be/vytjdqNpGUM`, where swing-up, stabilization and disturbance rejection are demonstrated.

5. CONCLUSION

This paper shows a scheme to achieve swing-up and stabilization of a CMG-actuated inverted pendulum. It is shown how a *divide and conquer* approach, by splitting the task of swing-up and stabilization, is able to achieve the task of controlling this complex nonlinear system using relatively simple LPV controllers. Further work concerns the investigation how the choice of LPV representation of the nonlinear system influences the controller design, and how this can be incorporated into the controller synthesis itself. The effects of more robust switching techniques on the system is also a topic open for research.

REFERENCES

Abbas, H.S., Ali, A., Hashemi, S.M., and Werner, H. (2013). LPV gain-scheduled control of a control moment gyroscope. In *Proc. of the American Control Conference*, 6841–6846. Washington, DC, USA.

Abbas, H.S., Ali, A., Hashemi, S.M., and Werner, H. (2014). LPV state-feedback control of a control moment gyroscope. *Control Engineering Practice*, 24, 129–137.

Apkarian, P., Gahinet, P., and Becker, G. (1995). Self-scheduled H_∞ control of linear parameter-varying systems: a design example. *Automatica*, 31(9), 1251–1261.

Åström, K. and Furuta, K. (2000). Swinging up a pendulum by energy control. *Automatica*, 36(2), 287–295.

Educational Control Products (1999). *Manual for Model 750 Control Moment Gyroscope*. Bell Canyon, CA, USA.

Educational Control Products (2003). *Manual for A51 Inverted Pendulum Accessory*. Bell Canyon, CA, USA.

Hjartarson, A., Seiler, P., and Packard, A. (2015). LPVTools: A toolbox for modeling, analysis, and synthesis of Parameter Varying control systems. *IFAC-PapersOnLine*, 48(26), 139–145.

Hoffmann, C. and Werner, H. (2015). A survey of linear parameter-varying control applications validated by experiments or high-fidelity simulations. *IEEE Transactions on Control Systems Technology*, 23(2), 416–433.

Kristiansen, R., Egeland, O., and Johan, P. (2005). A comparative study of actuator configurations for satellite attitude control. *Modeling, Identification and Control*, 26(4), 201–219.

Kurz, T., Eberhard, P., Henninger, C., and Schiehlen, W. (2010). From Neweul to Neweul-M2: symbolical equations of motion for multibody system analysis and synthesis. *Multibody System Dynamics*, 24(1), 25–41.

Jörgen Malmborg, Bo Bernhardsson, Karl Johan Åström, (1996). A Stabilizing Switching Scheme for Multi Controller Systems. In *IFAC Proceedings Volumes, Volume 29, Issue 1*, 2627–2632.

Packard, A. (1994). Gain scheduling via linear fractional transformations. *Systems and Control Letters*, 22(2), 79–92.

Perez, T. and Steinmann, P. (2008). Advances in gyrostabilization of vessel roll motion. In *Proc. of the Pacific International Maritime Conference*. Sydney, Australia.

Reyhanoglu, M. and van de Loo, J. (2006). State feedback tracking of a nonholonomic control moment gyroscope. In *Proc. of the 45th IEEE Conference on Decision and Control*, 6156–6161. San Diego, CA, USA.

Rugh, W.J. and Shamma, J.S. (2000). A survey of research on gain-scheduling. *Automatica*, 36, 1401–1425.

Scherer, C. (2001). LPV control and full block multipliers. *Automatica*, 27(3), 325–485.

Sefton, J. and Glover, K. (1990). Pole/zero cancellations in the general H_∞ problem with reference to a two block design. In *Systems & Control Letters*, 14(4), 295–306.

Theis, J., Radisch, C., and Werner, H. (2014). Self-scheduled control of a gyroscope. *IFAC-PapersOnLine*, 47(3), 6129–6134.

Wu, F. (1995). *Control of Linear Parameter Varying Systems*. Ph.D. thesis, University of California at Berkeley.